

AN EXPERIMENTAL STUDY OF DYNAMIC CHARACTERISTICS OF LABYRINTH SEAL

Takuzo Iwatsubo, Koji Fukumoto, and Hideyuki Mochida
Kobe University
Rokkodai-cho, Nada-ku
Kobe, Japan

512-37

12856

p. 19

Abstract

The fluid force due to labyrinth seal sometimes makes the turbomachineries unstable under higher rotating speed, higher pressure and higher power. Therefore, it is important to predict the magnitude and the direction of the fluid force and to evaluate the stability of the rotor system in design process.

Then, this paper shows the experimental results of the fluid force induced by a straight labyrinth seal and the rotordynamic coefficients calculated from the fluid force. Influences of the number of fins under the rotating speed, whirling speed, inlet pressure, inlet tangential velocity are mainly investigated on a stability of the rotor system.

The results show that increase of the number of fins makes the fluid force small and the rotor system stable, an increase of inlet pressure makes the fluid forces large and an increase of inlet tangential velocity makes the rotor system unstable.

Introduction

Labyrinth seal are used as the non-contact type seals between rotor and stator of the fluid turbomachineries, such as a gas turbine and a compressor. To improve the efficiency of these fluid turbomachineries, inlet pressure of the working fluid and rotating speed of the rotor tend to become higher while the clearance of labyrinth seal is designed narrow to prevent for the leakage flow. As the result of using such a high performance machineries, unstable vibrations of the rotor may occur and they may draw an industrial important problem. The labyrinth seal is considered as one of the cause of these vibration problems.

Unstable vibration induced by the labyrinth seal was first pointed out by Alford[1], and after that it has been studied by many investigators. Among them, Benckert & Wachter[2] had interested in the dynamic characteristics and they measured the hydraulic spring coefficients by using the static method. On the other hand, Wright[3] investigated the instability condition of rotors induced by the labyrinth seal force for two seal strips model under many test conditions and also measured the destabilizing fluid force which included the damping coefficient. Childs & Scharrer[4][5] presented the set of dynamic data in which inlet tangential velocity as well as vibratory frequency were adequately controlled. They reported directly measured force data for 16-tooth on stator seal and on rotor seal, and obtained good correlation to theory on the effect of some of the parameters. Scharrer[6] investigated the effect of the number of fins on the static and dynamic characteristics of labyrinth seals theoretically.

The Influences of the rotating speed, inlet pressure and inlet tangential velocity have been already investigated. But the influence of the number of fins have not been experimentally investigated yet. The purpose of this paper is to investigate the influences of the number of fins under the rotating speed, whirling speed, inlet pressure, inlet tangential velocity on a stability of the rotor system.

The fluid force is measured under the condition of both rotating and whirling motions of the rotor. The rotordynamic coefficients, which represent the flow induced force of labyrinth seal by the function of velocity and displacement, are obtained.

Test Facility

The test facility to measure the fluid force is shown in figure 1. In this figure the rotor is driven by the three-phase motor ⑨. The rotor is supported at the left and right sides by the eccentric bearings. The dimensions and directions of both eccentricities are set to be equal. Therefore, the rotor is whirled by the rotation of the eccentric bearing. The eccentric bearings are driven by the three-phase motor ⑩ through the timing-belt and pulley ⑪. Since the rotor and the eccentric bearing are driven by different motors, the rotor can be whirled in the same direction(forward) and in the opposite direction(backward), and these rotating and whirling speeds are continuously changed from 200(rpm) to 2000(rpm).

The working fluid is compressed by the compressor ⑭ and transported from the air-tank ⑬ into the test casing through the regulator ⑮. The test seals are changeable by changing seal ② and ③. The detail seal dimension in this test is shown in table 1.

The rotating speed of the rotor is measured by the pulse notched on the coupling. The whirling speed of the rotor is measured by the pulse of the balance weight ⑧.

The fluid forces generated in the labyrinth seal are measured by the pressure transducers as shown in figure 2 and six loadcells which directly support the seal as shown in figure 3. By measuring the force with six loadcells it is possible to measure the lateral force and moment. The measured signal current is sent to the AD converter through the D.C. amplifier and is analyzed. Figure 7 shows the data flow chart.

Analysis of Measured Data

Figure 4 shows the definition of displacement, velocity and flow induced forces.

(a) Data analysis of the pressure transducers

Since the data measured by the pressure transducers are the pressure distributions around the rotor, we can obtain the fluid forces by integrating the pressure distributions around and along the rotor.

It is assumed that the circumferential pressure distribution is elliptic and the center of it is O' as shown in figure 5. Thus, the circumferential pressure distribution in the i th chamber $P_i(\theta, t)$ is given as;

$$P_i(\theta, t) = \bar{P}_i + \Delta P_i \cdot \cos(\Omega t - \theta + \phi_i) \quad (1)$$

where \bar{P}_i is the magnitude of steady pressure in the i th chamber, ΔP_i is the magnitude of the pressure fluctuation in the i th chamber and ϕ_i is the phase of the fluid force relative to the rotor displacement. The x and y direction components of the fluid force in the i th chamber are obtained by using Eq.(1) and considering the condition that the eccentric direction of the rotor agrees with x direction, that is, $t = 0$, the following equations are obtained.

$$\begin{aligned} Fx_i &= - \int_0^{2\pi} P_i(\theta, t) \cdot Ptg \cdot Rs \cdot \cos \theta d\theta \\ &= -\pi \cdot Rs \cdot Ptg \cdot \Delta P_i \cos \phi_i \end{aligned} \quad (2)$$

$$\begin{aligned} Fy_i &= - \int_0^{2\pi} P_i(\theta, t) \cdot Ptg \cdot Rs \cdot \sin \theta d\theta \\ &= -\pi \cdot Rs \cdot Ptg \cdot \Delta P_i \sin \phi_i \end{aligned} \quad (3)$$

where Rs is the rotor radius, Ptg is the seal pitch. Then, since the overall fluid forces generated in the labyrinth seal are calculated by adding the fluid force in each chamber, the following equations are obtained.

$$Fx = -\pi \cdot Rs \cdot Ptg \cdot \sum_{i=1}^n \Delta P_i \cos \phi_i \quad (4)$$

$$Fy = -\pi \cdot Rs \cdot Ptg \cdot \sum_{i=1}^n \Delta P_i \sin \phi_i \quad (5)$$

where n is the number of fins.

(b) Data analysis of the loadcells

The fluid forces are calculated by dividing the each forces f_j , measured by six loadcells into x, y components and adding the divided force components in the each direction. That is to say, the fluid forces Fx, Fy is calculated by the following equations;

$$Fx = \frac{2}{3} \sum_1^6 f_j \cdot \cos(\alpha_j) \quad (6)$$

$$Fy = \frac{2}{3} \sum_1^6 f_j \cdot \sin(\alpha_j) \quad (7)$$

where α_j is each loadcell's setting angle.

Then, using these forces measured by loadcells, moment can be calculated.

Figure 6 shows the definition of the moment generated in the labyrinth seal. The moment are defined by Kanemori[9] as following equations;

$$Mx = (Fy_{in} - Fy_{out}) \cdot \frac{L_b}{2} \quad (8)$$

$$My = -(Fx_{in} - Fx_{out}) \cdot \frac{L_b}{2} \quad (9)$$

where M_x, M_y is the moment with regard to the x and y axes, respectively, $F_{x_{in}}, F_{y_{in}}$ are forces in x and y directions measured by inlet side loadcells, $F_{x_{out}}, F_{y_{out}}$ are forces in x and y directions measured by outlet side loadcells and L_b is the distance between the inlet side and the outlet side loadcells.

The rotordynamic coefficients are defined by the following equations.

$$-\begin{Bmatrix} F_x \\ F_y \end{Bmatrix} = \begin{bmatrix} K_{xx} & K_{xy} \\ K_{yx} & K_{yy} \end{bmatrix} \begin{Bmatrix} x \\ y \end{Bmatrix} + \begin{bmatrix} C_{xx} & C_{xy} \\ C_{yx} & C_{yy} \end{bmatrix} \begin{Bmatrix} \dot{x} \\ \dot{y} \end{Bmatrix} \quad (10)$$

where (x, y) are the rotor displacement, (F_x, F_y) are the x and y direction components of the reaction force acting on the rotor, and $(K_{xx}, K_{xy}, K_{yx}, K_{yy})$ and $(C_{xx}, C_{xy}, C_{yx}, C_{yy})$ are the stiffness and damping, respectively.

For small motion about a centered position, Eq.(10) is rewritten simpler as follows;

$$-\begin{Bmatrix} F_x \\ F_y \end{Bmatrix} = \begin{bmatrix} K_{xx} & K_{xy} \\ -K_{xy} & K_{xx} \end{bmatrix} \begin{Bmatrix} x \\ y \end{Bmatrix} + \begin{bmatrix} C_{xx} & C_{xy} \\ -C_{xy} & C_{xx} \end{bmatrix} \begin{Bmatrix} \dot{x} \\ \dot{y} \end{Bmatrix} \quad (11)$$

For centered position, the rotor displacement (x, y) are described as;

$$x = e \cos(\Omega t) \quad (12)$$

$$y = e \sin(\Omega t) \quad (13)$$

where e is the eccentricity of the rotor.

Substituting Eq.(12), Eq.(13) into Eq.(11) and considering the condition that the eccentric direction of the rotor agrees with x direction, that is, $t = 0$, the following equations are obtained.

$$-\frac{F_x}{e} = C_{xy}\Omega + K_{xx} \quad (14)$$

$$-\frac{F_y}{e} = C_{xx}\Omega - K_{xy} \quad (15)$$

$$F = \sqrt{F_x^2 + F_y^2} \quad , \quad \phi = \tan^{-1} \left(\frac{F_y}{F_x} \right) \quad (16)$$

where F is the magnitude of the fluid force.

As we obtain the fluid forces for 10 whirling speed Ω in experiments, we can determine the rotordynamic coefficients by the least squares method.

Experimental Results

The range of parameter in this test is shown in table 2. The ratio of inlet tangential velocity to rotor surface velocity (inlet tangential velocity ratio) is shown table 3. Figure 8 shows the comparison of the fluid force versus whirling/ rotating ratio between the loadcell data and the pressure transducer data. This figure also shows the magnitude and the phase of the fluid force measured by two ways almost agree. After this, the data put in this paper are the one measured by the loadcells.

Fluid Forces and Moment Results

Figure 9 shows an effect of the rotating speed on the fluid force changing whirling/rotating speed. The figure shows that the tangential force, F_y , is sensitive to the change of rotating speed. The figure also shows that the radial force, F_x , changes very much from negative to positive with increasing the number of fins and is constant with increasing the rotating speed.

Figure 10 shows an effect of the inlet pressure on the fluid force changing whirling/rotating speed. The figure shows that the tangential force, F_y , increases with increasing inlet pressure and the radial force, F_x , increases the magnitude with increasing inlet pressure. The figure also shows that the tendencies of the tangential force and the radial force to the number of fins is constant.

Figure 11 shows an effect of the inlet tangential velocity on the fluid force changing whirling/rotating speed. The figure shows that the tangential force, F_y , increases from negative to positive with increasing the inlet tangential velocity from negative to positive and the radial force F_x changes the slope from right-up to right-down with increasing the inlet tangential velocity. As shown in figure 13 which are calculated results, inlet tangential velocity has a greater influence on the seal which have less seal fins.

Figure 12 shows an effect of the number of fins on the fluid force changing whirling/rotating speed. The figure shows that the tangential force, F_y , is sensitive to inlet tangential velocity with decreasing the number of fins, the radial force, F_x , increases from the negative to positive with increasing the number of fin in every inlet tangential velocity.

Figure 14 shows an effect of rotating speed on the moment changing whirling/rotating speed. The figure shows that the moment with regard to the x axis, M_x , is constant with increasing the rotating speed and the number of fins, the moment with regard to the y axis, M_y , is constant with increasing the rotating speed and the magnitude of M_y increases with increasing the number of fins.

Figure 15 shows an effect of the inlet pressure on the moment changing whirling/rotating speed. The figure shows that the moment with regard to the x axis, M_x , is constant with increasing the inlet pressure and the number of fins, the magnitude of moment with regard to the y axis, M_y , increases with increasing the number of fins.

Figure 16 shows an effect of the inlet tangential velocity on the moment changing whirling/rotating speed. The figure shows that the moment with regard to the x axis changes negative to positive with increasing the inlet tangential velocity in every seal, the magnitude of moment with regard to the y axis increases with increasing the number of fins.

Figure 17 shows an effect of the number of fins on the moment changing whirling/rotating speed. The figure shows that the moment with regard to the x axis changes negative to positive with increasing the inlet tangential velocity, the moment with regard to the y axis changes very much with increasing the number of fins.

Rotordynamic Coefficients Results

Figure 18 show that an effect of the number of fins on the rotordynamic coefficients changing the inlet pressure.

The figure 18(a) shows that the magnitude of direct stiffness increases with increasing inlet pressure. This figure also shows that direct stiffness changes positive to negative with increasing the number of fins.

The figure 18(b) shows that an increase of inlet pressure makes the magnitude of cross-coupled stiffness large. This figure also shows that the magnitude of cross-coupled stiffness decreases with increasing the number of fin.

The figure 18(c) shows that direct damping increases with increasing inlet pressure.

The figure 18(d) shows that an increase of inlet pressure has no influence on cross-coupled damping. The magnitude of cross-coupled damping increases with increasing the number of fins.

Figure 19 show that an effect of the number of fins on the rotordynamic coefficients changing the inlet tangential velocity.

The figure 19(a) shows that a change of inlet tangential velocity has no influence on direct stifness. The figures also show that direct stiffness changes from positive to negative with increasing the number of fins.

The figure 19(b) shows that cross-coupled stiffness changes from negative to positive with increasing inlet tangential velocity, and the quantity of cross-coupled stiffness fluctuation in this time is greater with decreasing the number of fins.

The figure 19(c) shows that direct damping is constant with increasing inlet tangential velocity.

The figure 19(d) shows that cross-coupled damping changes from negative to positive with increasing inlet tangential velocity and the quantity of cross-coupled damping fluctuation in this time is greater with decreasing the number of fins.

Figure 20 shows that an effect of the number of fins on 'whirl frequency ratio' changing the inlet tangential velocity.

Whirl frequency ratio f is defined by Childs[4] as following equation;

$$f = \frac{K_{xy}}{C_{xx}\Omega}$$

where Ω is rotor whirling frequency, $K_{xy}/C_{xx}\Omega$ is the ratio of the destabilizing influence of the cross-coupled stiffness and the stabilizing influence of direct damping. From viewpoint of stability, a less value of whirl frequency ratio is desirable.

The figure shows that 11 fin's labyrinth seal has a greater whirl ratio than other seals in giving inlet tangential velocity. And this agrees with Scharrer's theoretical results[6].

Conclusion

In this paper, the fluid force, moment and the rotordynamic coefficients are experimentally obtained. The conclusions are as follows;

1. The labyrinth seal which has less seal fins is sensitive to increase of inlet tangential velocity.

2. The labyrinth seal which has less seal fins is not always stable.
3. Tangential fluid force increases with increasing inlet pressure and inlet tangential velocity.
4. Radial fluid force increases the magnitude with increasing inlet pressure.
5. Moment with regard to the x axis is sensitive to the change of inlet tangential velocity.
6. Moment with regard to the y axis increases the magnitude with increasing the number of fins.
7. Cross-coupled damping and stiffness increases from negative to positive with increasing inlet tangential velocity.
8. Direct damping is constant with increasing inlet tangential velocity.

References

1. Alford, J.S. : " Protecting Turbomachinery from Self-Excited Rotor Whirl " Trans. ASME, J. Eng. Power, Oct. 1965, pp. 333-344
2. Benckert, H. ;and Wachter, J. : " Flow Induced Spring Coefficients of Labyrinth Seals for Application in Rotor Dynamics " NASA Lewis, Conference Publication 2133, Rotordynamic Instability Problems in High-Performance Turbomachinery, 1980, pp. 189-212
3. Wright, D.V. : " Air Model Tests of Labyrinth Seal Force on Whirling Rotor " Trans. ASME, J. Eng. Power, Oct. 1978, pp. 533-543
4. Childs, D.W.;and Scharrer, J.K. : " Experimental Rotordynamic Coefficient Results for Teeth-on-Rotor and Teeth-on-Stator Labyrinth Gas Seals " Trans. ASME, J. Eng. Gas Turbines Power, Oct. 1986, pp. 599-604
5. Childs, D.W. ;and Scharrer, J.K. : " Theory Versus Experiment for the Rotordynamic Coefficients of Labyrinth Gas Seals: Part 2 - A Comparison to Experiment ", Trans. ASME, J. Vib. Acoust. Stress Reliab. Des., July 1988, pp.281-287
6. Scharrer, J.K. : " Rotordynamic Coefficients for Stepped Labyrinth Gas Seals ", Rotordynamic Instability Problems in High-Performance Turbomachinery 1988, pp.177-195
7. Kanemitsu, Y. ;and Osawa, M. : " Cross-Coupled Aerodynamic Forces on a Whirling Rotor of Labyrinth Seals (Straight-Type Labyrinth Seals) " Trans. JSME, Vol.51, No.472 , Dec. 1985, pp. 3407-3412
8. Kanemitsu, Y. ;and Osawa, M. : " Cross-Coupled Aerodynamic Forces on a Whirling Rotor of Labyrinth Seals (2nd Report, Interlocking-type Seals) " Trans. JSME, Vol.54, No.498 , Feb. 1988, pp. 346-352

9. Kanemori, Y. ;and Iwatsubo, T. : " Expeimental Study of the Dynamic Characteristics of a Long Annular Seal (Fluid Force due to Conical and Cylindrical Whirl) " (in Japanese) Trans. JSME, Vol.56, No.532 , Dec. 1990, pp. 56-64
10. Iwatsubo, T. ;and Sugimaru, N. : " Experiment for Unstable Fluid Force in Labyrinth Seals " (in Japanese) Trans. JSME, No.910-39 Vol.B , Jul. 1991, pp. 202-206

Table.1 Seal Dimension in this study

Seal Clearance	mm	0.5
Fin Height	mm	4.0
Seal Pitch	mm	6.0
Fin Thickness	mm	1.0
Rotor Radius	mm	80.0
Number of Fin		5,11,21
Fin Side		On Stator

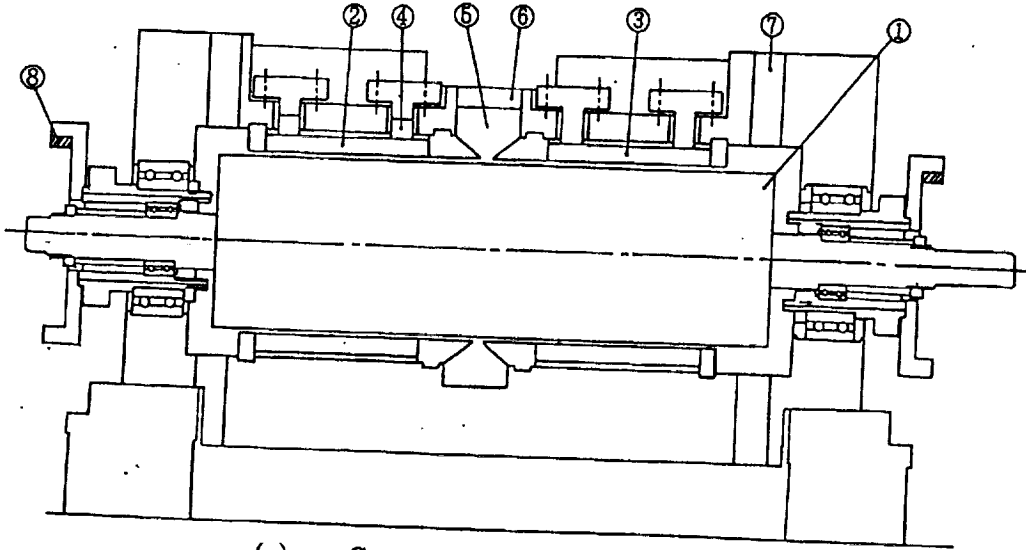
Table.2 Experiment Condition

Rotating Speed	ω (rpm)	1000 , 1500 , 2000
Whirling Speed	Ω (rpm)	$\pm (0.2 , 0.4 , 0.6 , 0.8 , 1.0) \times \omega$
Inlet Pressure	P_{in} (MPa)	0.2 , 0.3 , 0.4
Inlet Tangential Velocity	w_{in} (m/s)	-34.0 , 0 , 34.0

Table 3 Preswirl Velocity Ratio

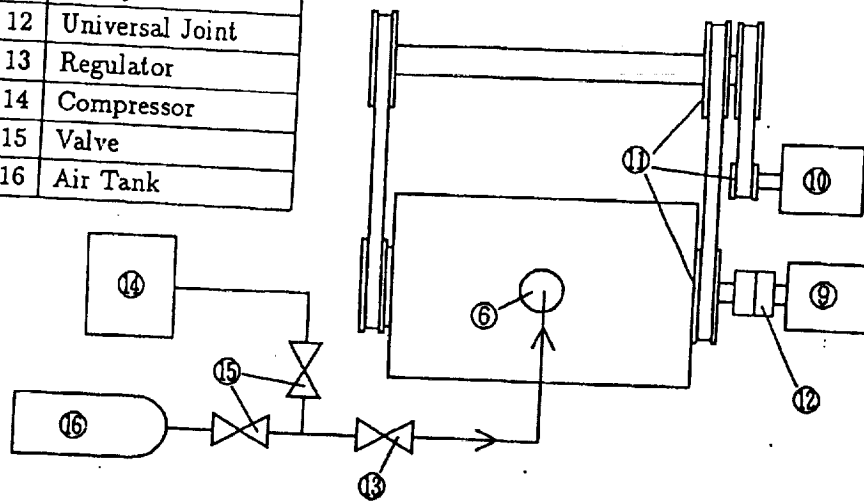
	-34.0(m/s)	0(m/s)	34.0(m/s)
1000(rpm)	-4.06	0.0	4.06
1500(rpm)	-2.70	0.0	2.70
2000(rpm)	-2.03	0.0	2.03

1	Rotor	4	Loadcell
2	Labyrinth Seal (on stator)	5	Swirl Chamber
3	Labyrinth Seal (on rotor)	6	Air Entrance
		7	Air Exit
		8	Balance Weight



(a) Cross section of test facility

9	Three-phase Motor (for rotation)
10	Three-phase Motor (for whirl)
11	Timing-belt and Pulley
12	Universal Joint
13	Regulator
14	Compressor
15	Valve
16	Air Tank



(b) Test facility layout

Fig. 1 Test facility

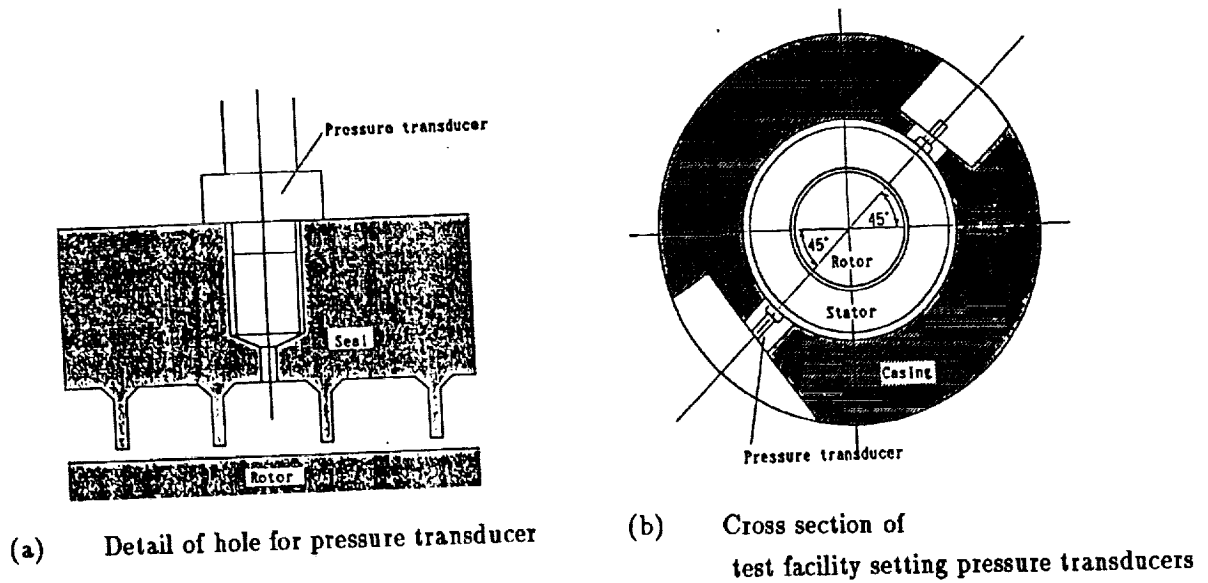


Fig. 2 Setting of pressure transducer

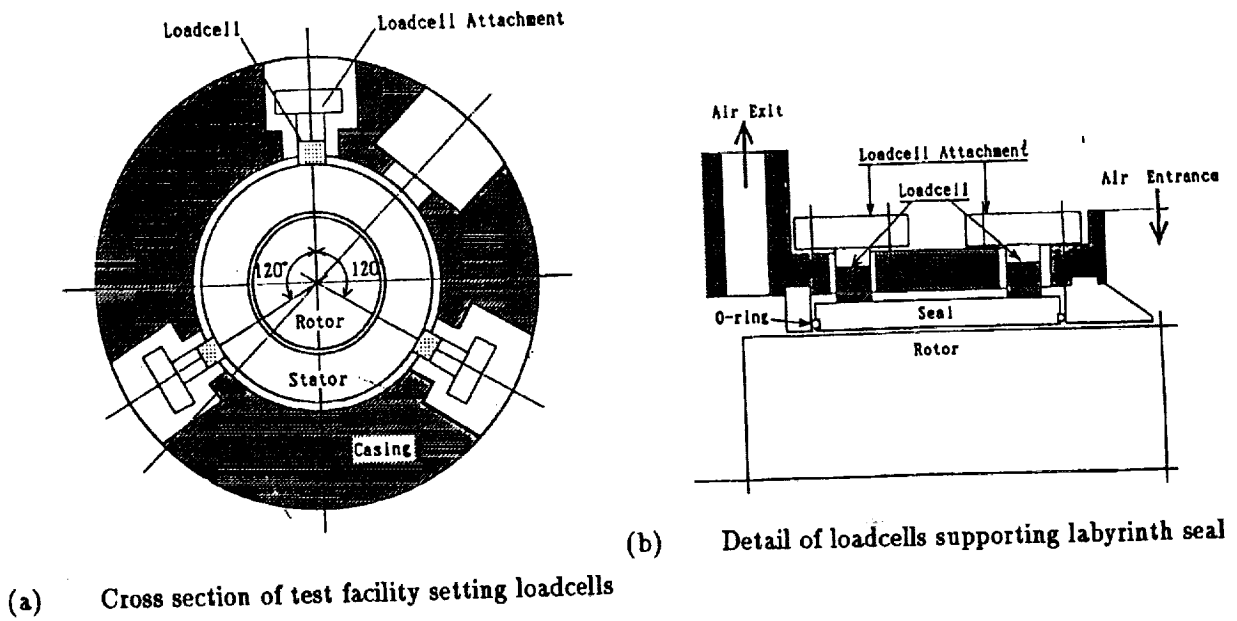


Fig. 3 Setting of loadcells

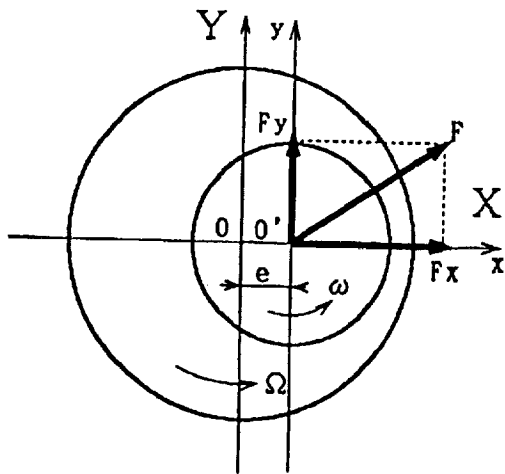


Fig. 4 Definition of displacement, velocity and flow induced force

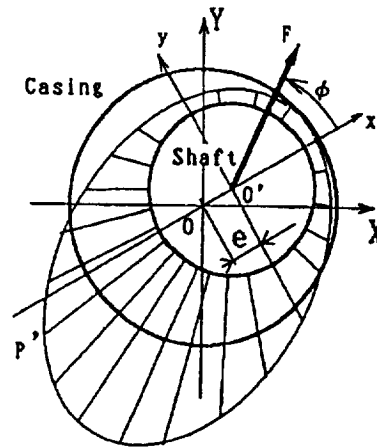


Fig. 5 Pressure distribution around the rotor

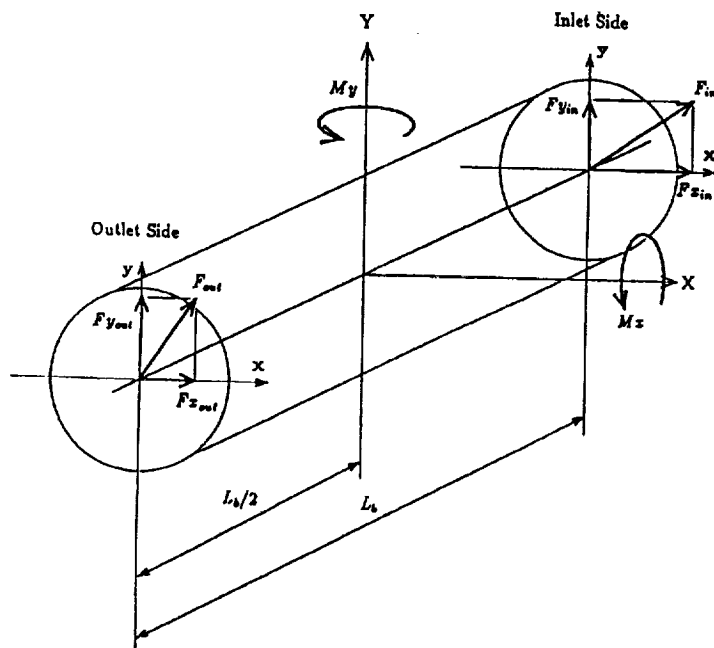


Fig. 6 Definition of flow induced force and moment

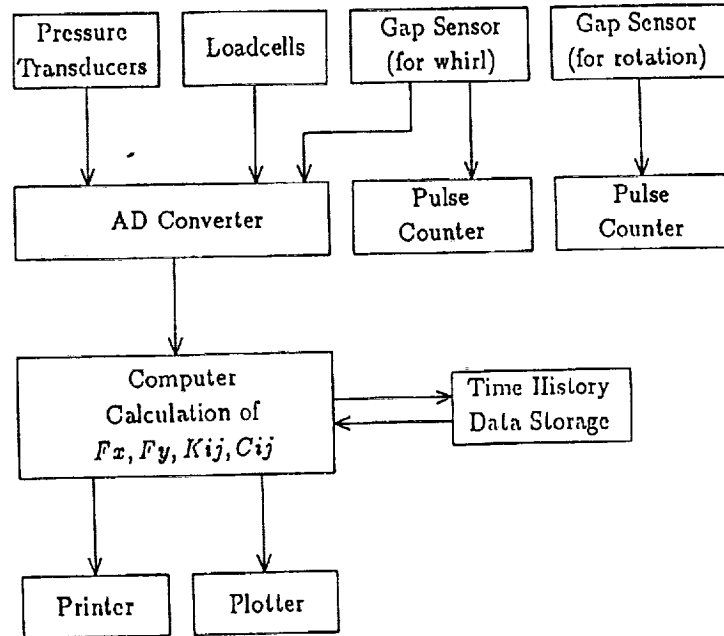


Fig. 7 Data flow chart

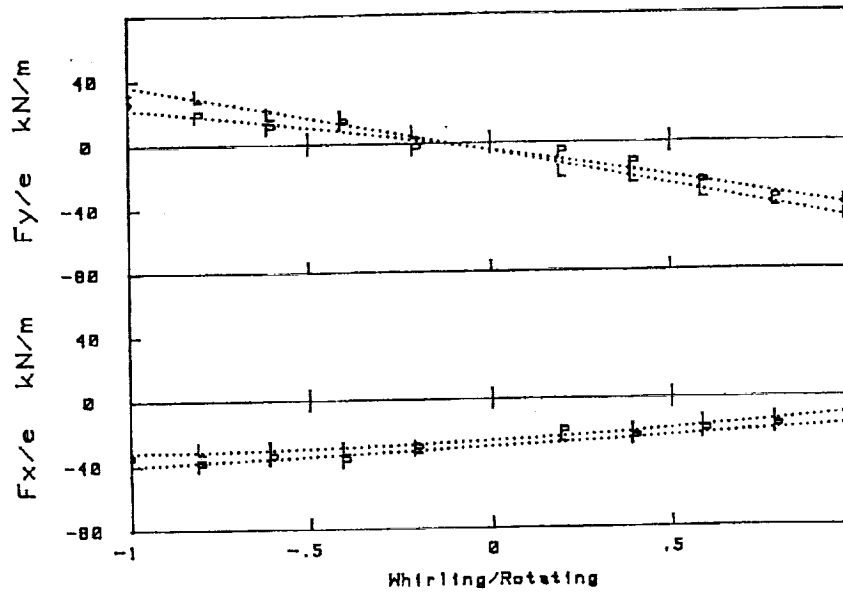
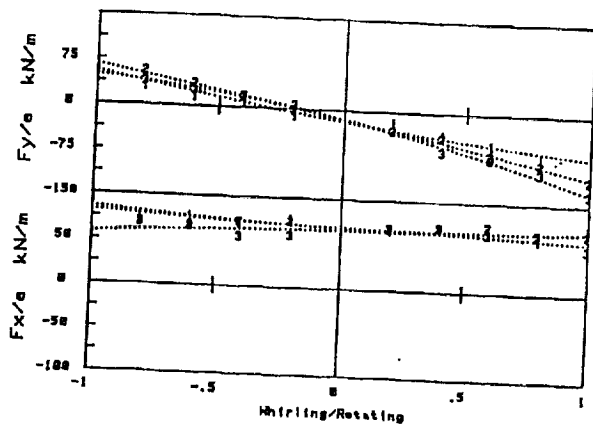


Fig. 8 Comparison of loadcells data and pressure transducers data

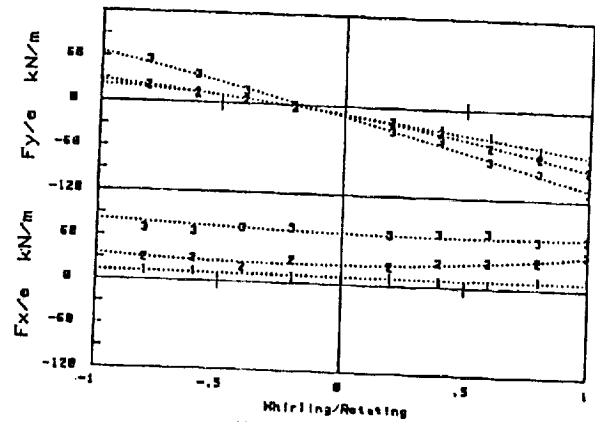
$\omega = 2000$ (rpm) , $P_{in} = 0.1$ (MPa) , $w_{in} = 0$ (m/s)

L : Loadcells data

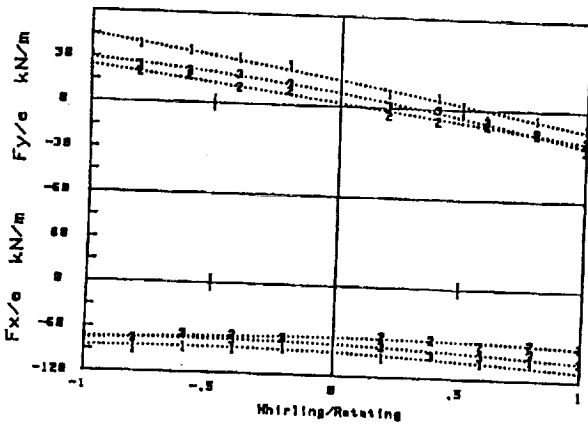
P : Pressure transducers data



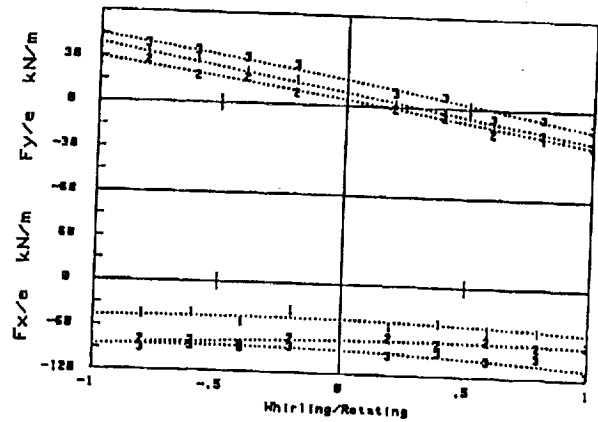
(a) 21 fins



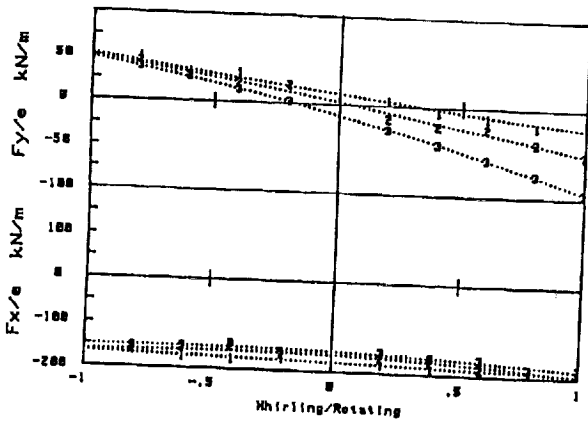
(a) 21 fins



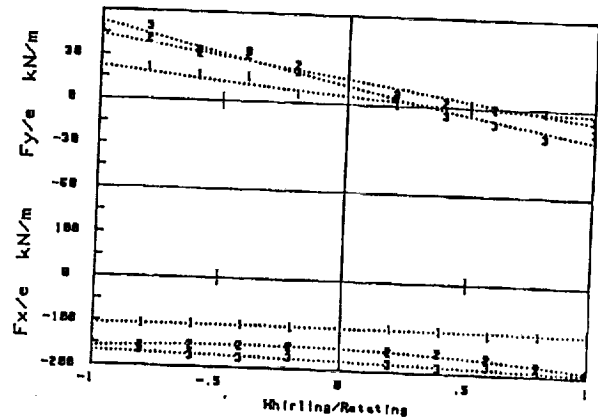
(b) 11 fins



(b) 11 fins



(c) 5 fins



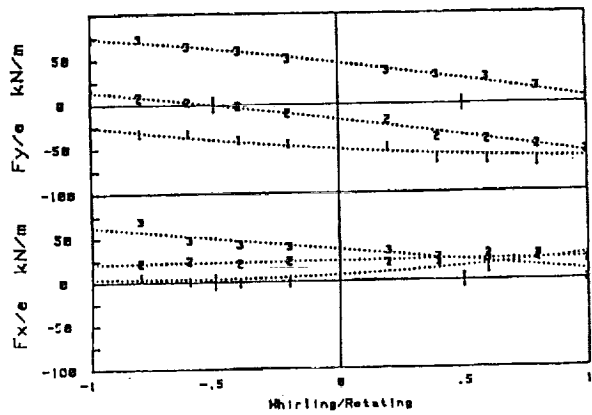
(c) 5 fins

Fig. 9 Fluid force versus whirling/rotating ratio
(Parameter: Rotating speed)
 $P_{in} = 0.4$ (MPa), $w_{in} = 0$ (m/s)

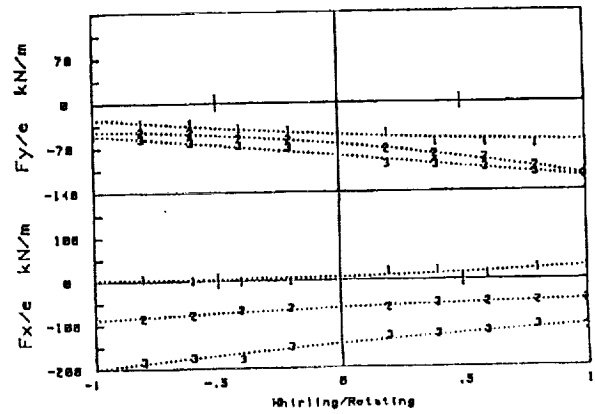
- 1 : 1000(rpm)
- 2 : 1500(rpm)
- 3 : 2000(rpm)

Fig. 10 Fluid force versus whirling/rotating ratio
(Parameter: Inlet Pressure)
 $\omega = 1000$ (rpm), $w_{in} = 0$ (m/s)

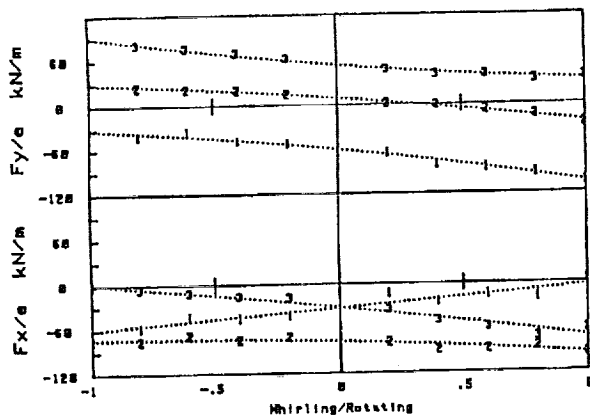
- 1 : 0.2 (MPa)
- 2 : 0.3 (MPa)
- 3 : 0.4 (MPa)



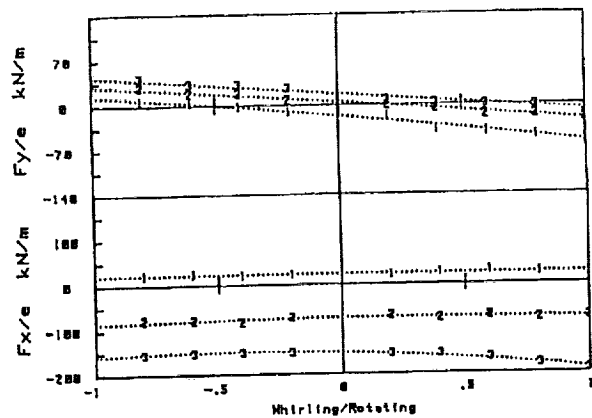
(a) 21 fins



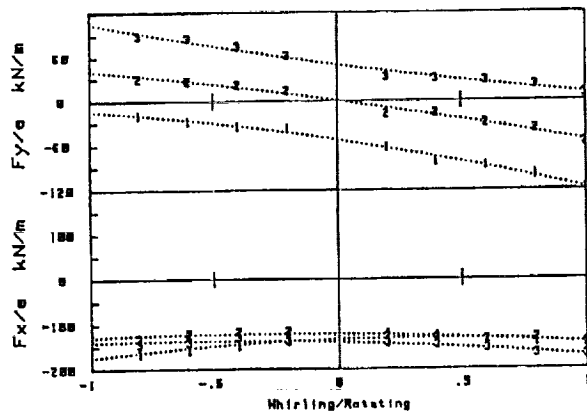
(a) $w_{in} = -34.0$ (m/s)



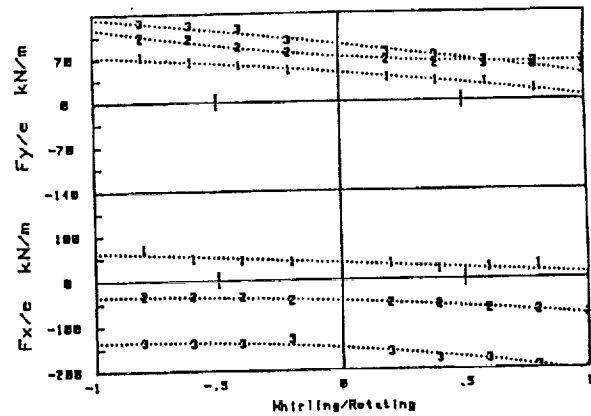
(b) 11 fins



(b) $w_{in} = 0.0$ (m/s)



(c) 5 fins



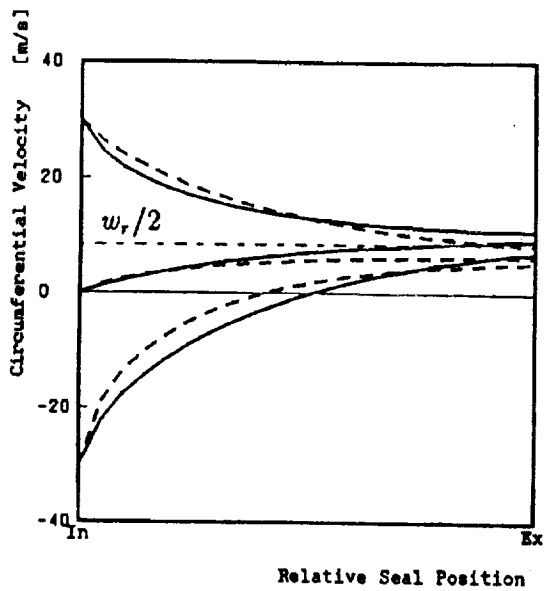
(c) $w_{in} = 34.0$ (m/s)

Fig. 11 Fluid force versus whirling/rotating ratio
(Parameter: Inlet tangential velocity)
 $\omega = 2000$ (rpm), $P_{in} = 0.2$ (MPa)

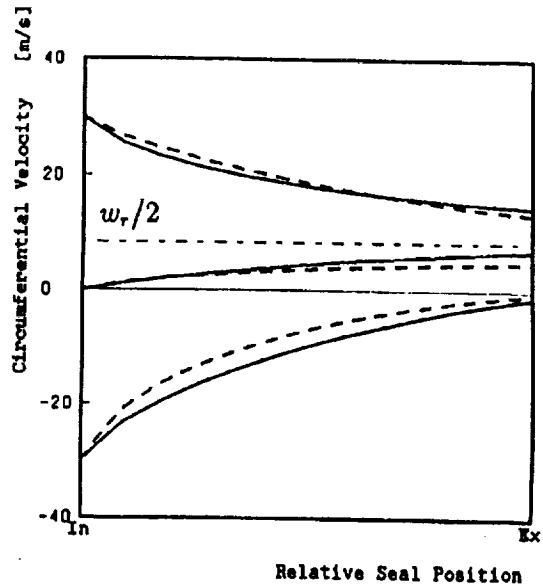
Fig. 12 Fluid force versus whirling/rotating ratio
(Parameter: The number of fins)
 $\omega = 1000$ (rpm), $P_{in} = 0.3$ (MPa)

1 : -34.0 (m/s)
2 : 0.0 (m/s)
3 : 34.0 (m/s)

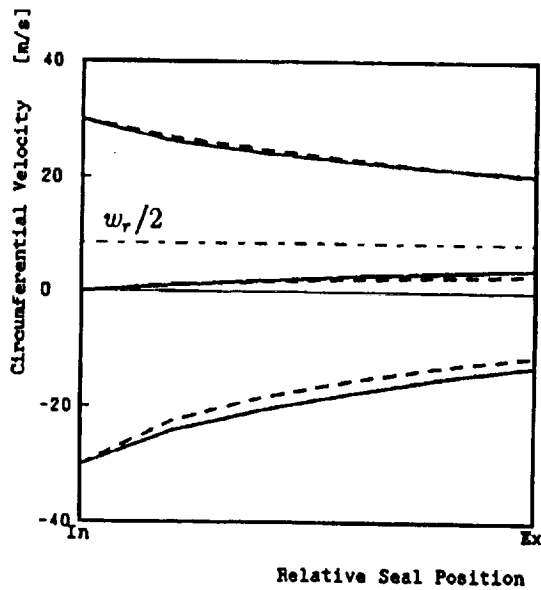
1 : 21 fins
2 : 11 fins
3 : 5 fins



(a) 21 fins



(b) 11 fins

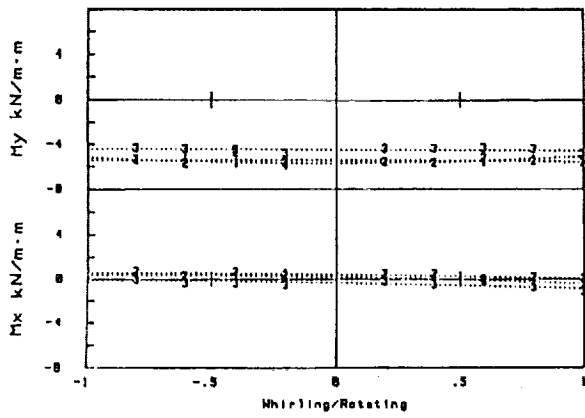


(c) 5 fins

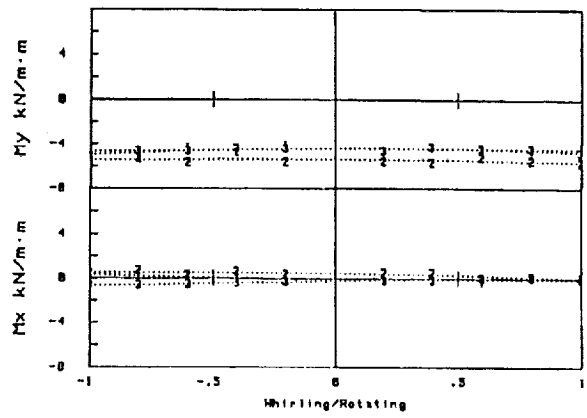
Fig. 13 Circumferential velocity versus seal length
 (Parameter: fin side)
 $\omega = 2000$ (rpm) , $P_{in} = 0.3$ (MPa)

———— Teeth on stator
 - - - - - Teeth on rotor

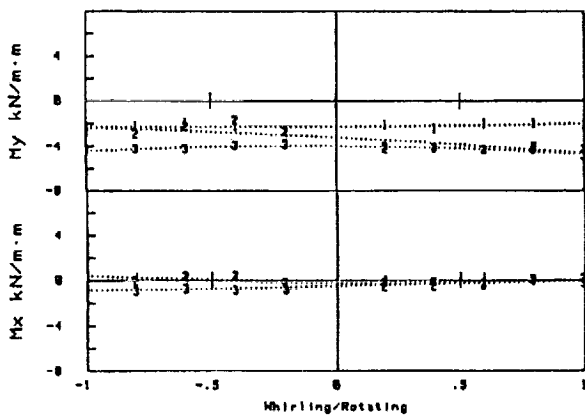
w_r : Rotor surface speed



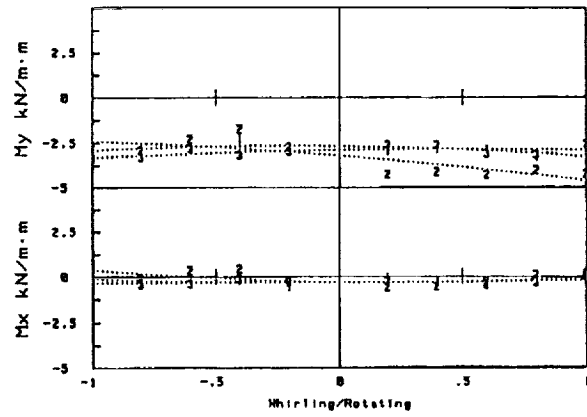
(a) 21 fins



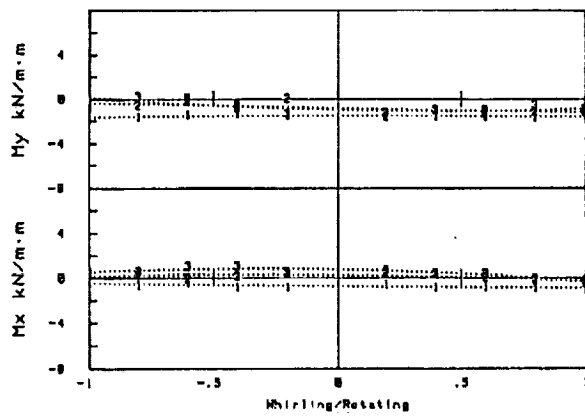
(a) 21 fins



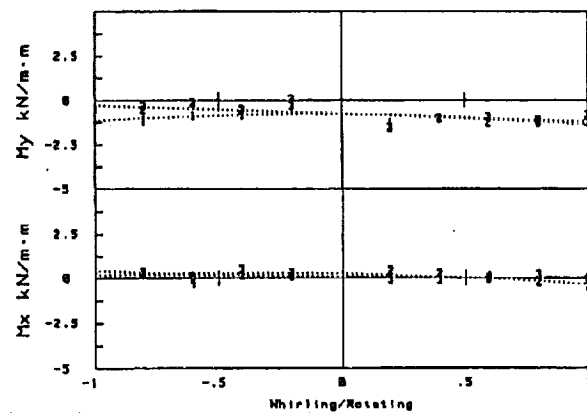
(b) 11 fins



(b) 11 fins



(c) 5 fins



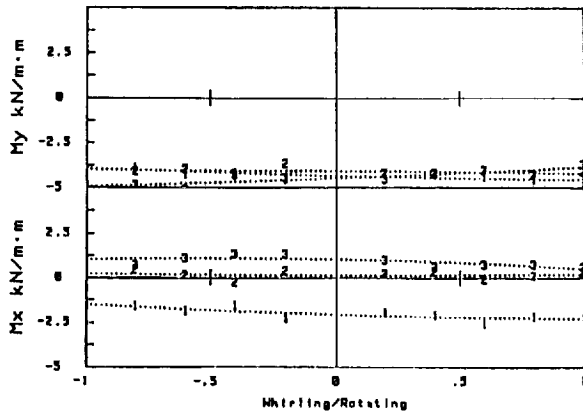
(c) 5 fins

Fig. 14 Moment versus whirling/rotating ratio
(Parameter: Rotating speed)
 $P_{in} = 0.3$ (MPa), $w_{in} = 0$ (m/s)

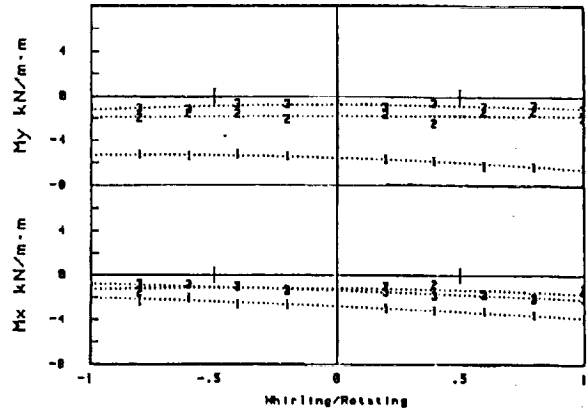
- 1 : 1000(rpm)
- 2 : 1500(rpm)
- 3 : 2000(rpm)

Fig. 15 Moment versus whirling/rotating ratio
(Parameter: Inlet pressure)
 $\omega = 1500$ (rpm), $w_{in} = 0$ (m/s)

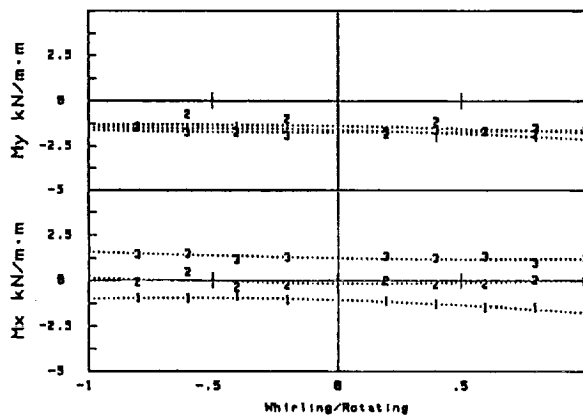
- 1 : 0.2 (MPa)
- 2 : 0.3 (MPa)
- 3 : 0.4 (MPa)



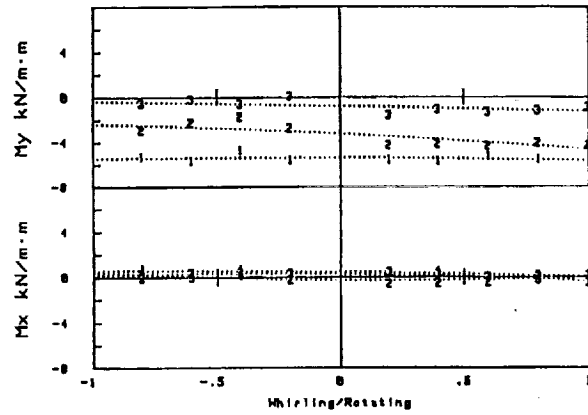
(a) 21 fins



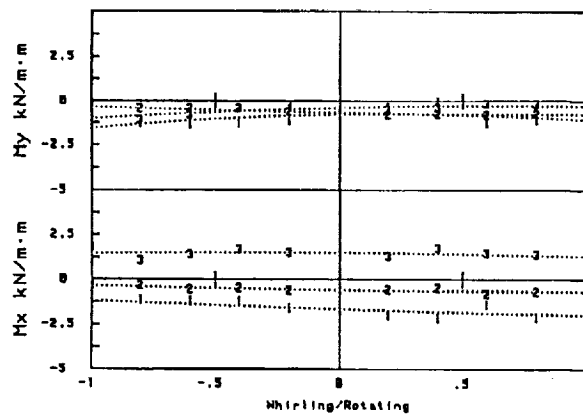
(a) $w_{in} = -34.0$ (m/s)



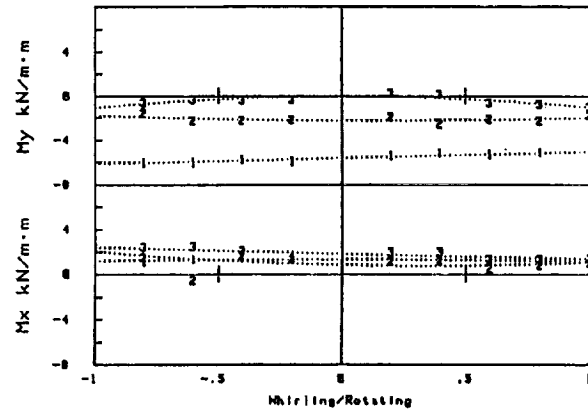
(b) 11 fins



(b) $w_{in} = 0.0$ (m/s)



(c) 5 fins



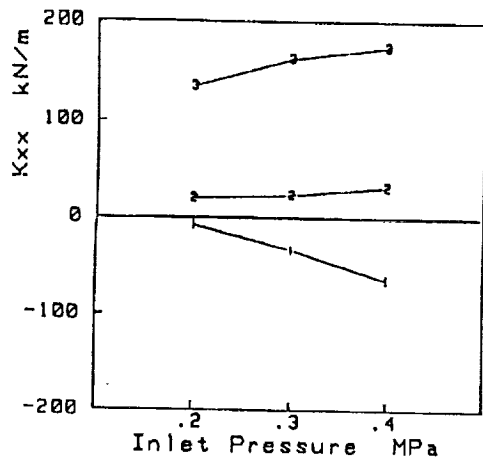
(c) $w_{in} = 34.0$ (m/s)

Fig. 16 Moment versus whirling/rotating ratio
(Parameter: Inlet tangential velocity)
 $\omega = 1000$ (rpm), $P_{in} = 0.2$ (MPa)

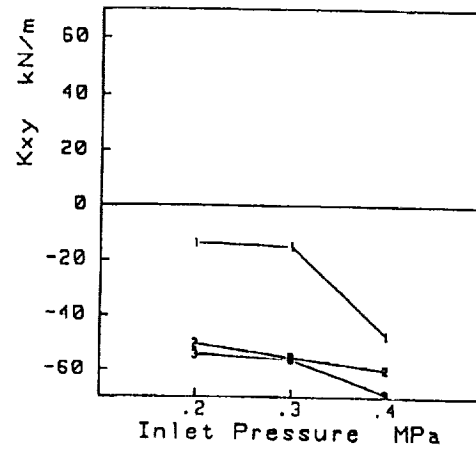
- 1 : -34.0 (m/s)
- 2 : 0.0 (m/s)
- 3 : 34.0 (m/s)

Fig. 17 Moment versus whirling/rotating ratio
(Parameter: The number of fins)
 $\omega = 1500$ (rpm), $P_{in} = 0.3$ (MPa)

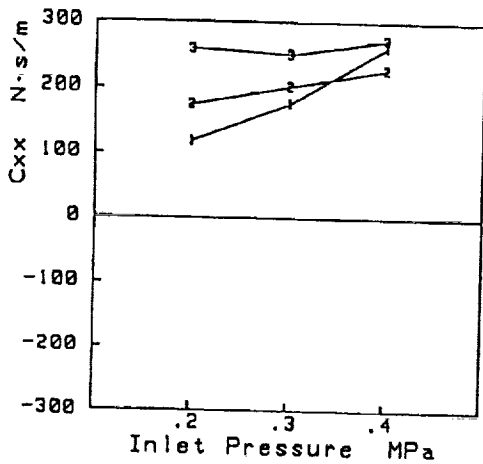
- 1 : 21 fins
- 2 : 11 fins
- 3 : 5 fins



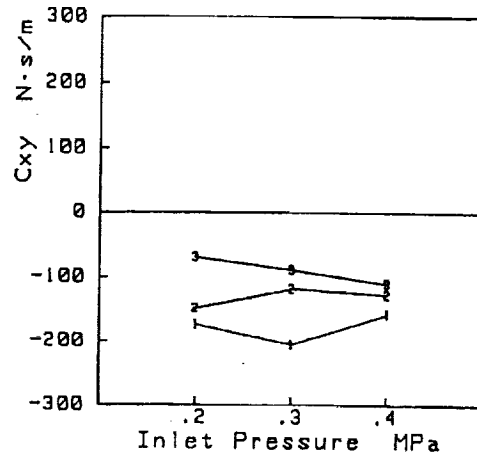
(a) Direct stiffness versus inlet pressure



(b) Cross-coupled stiffness versus inlet pressure



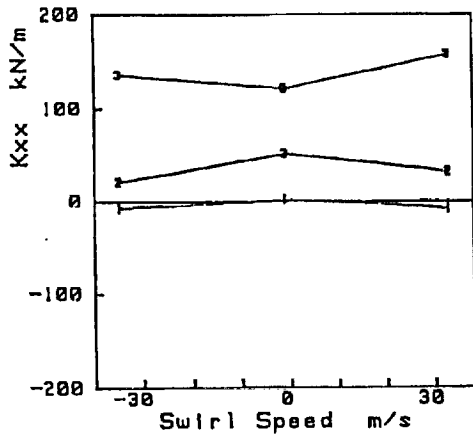
(c) Direct damping versus inlet pressure



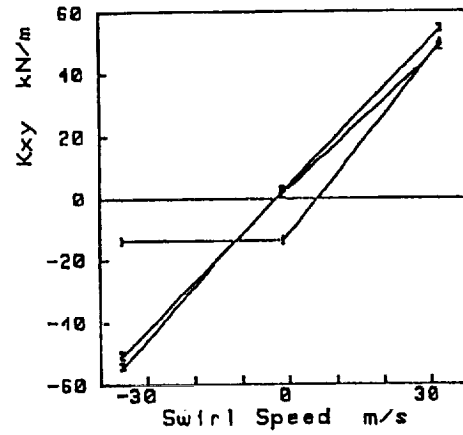
(d) Cross-coupled damping versus inlet pressure

Fig. 18 Rotordynamic coefficients versus inlet pressure
 (Parameter: The number of fins)
 $\omega = 2000$ (rpm), $w_{in} = -34.0$ (m/s)

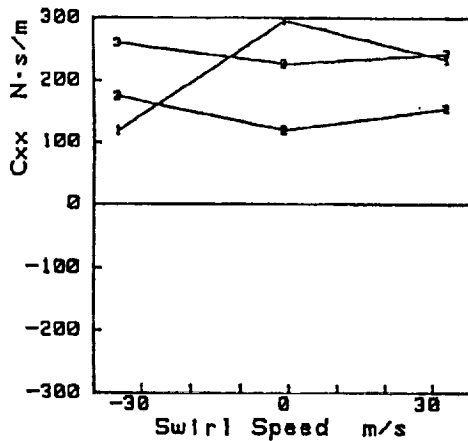
- 1 : 21 fins
- 2 : 11 fins
- 3 : 5 fins



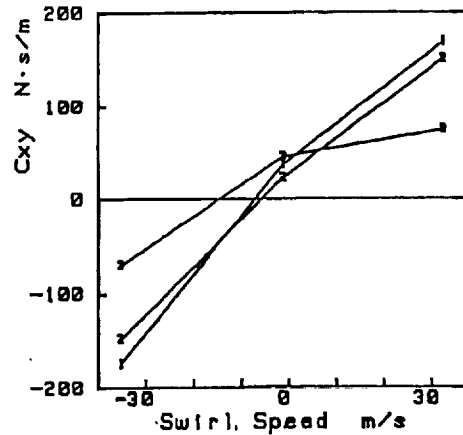
(a) Direct stiffness versus inlet tangential velocity



(b) Cross-coupled stiffness versus inlet tangential velocity



(c) Direct damping versus inlet tangential velocity



(d) Cross-coupled damping versus inlet tangential velocity

Fig. 19 Rotordynamic coefficients versus inlet tangential velocity

(Parameter: The number of fins)
 $\omega = 2000$ (rpm), $P_{in} = 0.2$ (MPa)

1	: 21 fins
2	: 11 fins
3	: 5 fins

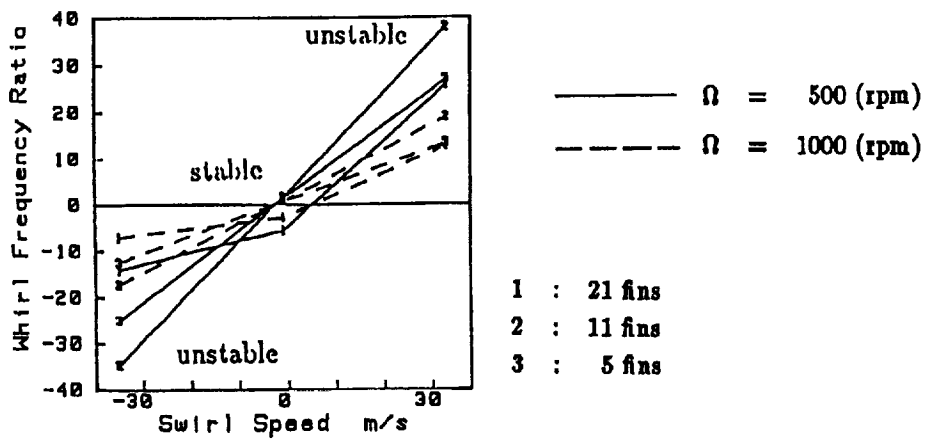


Fig. 20 Whirl frequency ratio versus inlet tangential velocity

(Parameter: The number of fins)
 $\omega = 2000$ (rpm), $P_{in} = 0.2$ (MPa)

